Geophysical Research Letters

RESEARCH LETTER
10.1029/2024GL112027

Statistical Characteristics of Wavelike Banded Convection Associated With Ducted Gravity Waves Over Southern China

Xuan Zhou[1,2,3], Yu Du[1,2,3], Junhong Wei[1,2,3], Zijin Chen[1,2,3], and Hongpei Yang[1,2,3]

[1]School of Atmospheric Sciences, Sun Yat-Sen University, and Southern Marine Science and Engineering Guangdong Laboratory (Zhuhai), Zhuhai, China, [2]Guangdong Province Key Laboratory for Climate Change and Natural Disaster Studies, Sun Yat-Sen University, Zhuhai, China, [3]Key Laboratory of Tropical Atmosphere-Ocean System, Sun Yat-Sen University, Ministry of Education, Zhuhai, China

Key Points:

- Distinct differences exist between wavelike banded convection with and without the presence of a wave duct
- Wavelike banded convection associated with ducted gravity waves is most likely to occur on winter or spring nights
- The phase speeds of these bands show a positive correlation with the depth of the ducting layer, consistent with wave ducting theory

Correspondence to:

Y. Du and J. Wei,
duyu7@mail.sysu.edu.cn;
weijunh@mail.sysu.edu.cn

Citation:

Zhou, X., Du, Y., Wei, J., Chen, Z., & Yang, H. (2024). Statistical characteristics of Wavelike banded convection associated with ducted gravity waves over Southern China. *Geophysical Research Letters*, *51*, e2024GL112027. https://doi.org/10.1029/2024GL112027

Received 16 AUG 2024
Accepted 8 OCT 2024

Abstract Wavelike banded convection occurs frequently and persistently in southern China, significantly impacting local weather. This study presents the first multi-year investigation of wavelike banded convection associated with ducted gravity waves in southern China from 2013 to 2021 using radar mosaic maps. These convective bands are highly dependent on the wave ducting environment, which typically exhibits a three-layer stratification structure. Out of 112 identified cases, two types were further classified based on the presence of a wave ducting vertical structure in the soundings: WaveDuct and nonWaveDuct type. Unlike nonWaveDuct type, the WaveDuct type predominantly happens on winter or spring nights. The phase speeds of WaveDuct convective bands also show a highly positive correlation with the depth of the ducting layer, consistent with wave ducting theory. This study provides a climatological understanding of the frequencies, movements, and environment conditions of wavelike banded convection related to ducted gravity waves over southern China.

Plain Language Summary In southern China, convective morphology sometimes exhibits wavelike banded features, which can persist for extended period. Recent studies show that the interaction between ducted gravity waves and convection organizes convection into wavelike banded patterns, and their long-lived propagation characteristic has a sustained impact on weather conditions. While previous research has primarily focused on case studies in southern China, this study further statistically examines the temporal and spatial distribution characteristics of wavelike banded convection associated with ducted gravity waves in southern China, offering a broader understanding of these phenomena.

1. Introduction

Gravity waves are widespread atmospheric phenomena associated with significant and disruptive weather changes (Koppel et al., 2000). Various mechanisms can generate gravity waves, including jet imbalance (Wei & Zhang, 2014, 2015; Zhang, 2004), shear flow (Bretherton, 1988; Lin & Chun, 1991), terrain (Starr Malkus & Stern, 1953; Tjernström & Mauritsen, 2009), convection (Lin & Goff, 1988; Yang & Du, 2024; Yang et al., 2023, 2024), and differences in heating between land and sea (Chen & Du, 2024; Du, 2023; Du et al., 2019; Du & Rotunno, 2015, 2018; Fang & Du, 2022; Lin & Smith, 1986; Rotunno, 1983; Sun & Orlanski, 1981). Convection plays a crucial role in gravity wave generation (Alexander et al., 1995; Bosart & Cussen, 1973; Du et al., 2024; Lin & Goff, 1988; Stephan et al., 2016) and often couples with gravity waves to produce wavelike banded convection (Du & Zhang, 2019; Ruppert et al., 2022). The wavelike convective bands have been observed and simulated worldwide, including phenomena such as the "morning glory cloud" in Australia (Clarke, 1972), cloud bands during snow bomb event in northeastern United States (Bosart et al., 1998), across the conterminous United States (Koppel et al., 2000), and banded convective activities in southern China (Du et al., 2021; Du & Zhang, 2019).

The coexistence of "wave-CISK (conditional instability of the second kind)" and "wave ducting" mechanisms effectively explain the propagation and maintenance of organized mesoscale convective bands (Koch et al., 2001; Powers & Reed, 1993; Zhang et al., 2001). The term "wave-CISK" was originally introduced by Lindzen (1974) and Raymond (1975) to describe the process where low-level convergence generated by gravity waves triggers latent heat release, with gravity waves responding positively to the latent heating and further influencing convection. Subsequent research has expanded the wave-CISK concept to encompass the interaction between gravity

waves and convection (Koch et al., 1988; Lane & Zhang, 2011; Lindzen, 1974; Powers, 1997; Raymond, 1984, 1987; Zhang et al., 2001).

Wave ducting is a classical theory conceptualized by Lindzen and Tung (1976) to explain the maintenance of long-lived horizontally propagating gravity waves. It involves a stable low-level layer acting as the primary medium for gravity wave propagation and an overlying reflecting layer with negligible static stability, which effectively redirects wave energy downwards (Ruppert et al., 2022). This reflective layer often forms around a critical level where the horizontal ground-relative phase velocity of the wave matches the background horizontal wind component (U) in the direction of wave propagation, with a Richardson number (Ri) less than 0.25 (Rottman & Einaudi, 1993). The ducting layer often appears as a thermal inversion layer, while the reflecting layer is statically neutral and/or conditionally unstable (Lindzen & Tung, 1976; Uccellini & Koch, 1987).

Uccellini and Koch (1987) conducted an observational review based on 13 documented long-lived lower tropospheric gravity wave events, and they noted that the observed phase speeds of large-amplitude mesoscale gravity waves are in good agreement with theoretical expectations from the Lindzen and Tung (1976) ducted gravity wave model. The large-amplitude mesoscale gravity waves are also long-lived (6–12hr) and can be associated with dynamical features such as singular waves of depression or wave packets with periods of a few hours. In addition, Koppel et al. (2000) presented results of a 25-year climatology of inertia–gravity waves (IGWs) from large-amplitude hourly surface pressure changes across the conterminous United States using a network of hourly surface airways observations (SAOs). The analysis shows IGWs occurrences are most likely seasonally in winter and spring and most common across the Great Plains and from the Great Lakes toward western New England.

Mesoscale convective systems (MCSs) in Southern China sometimes exhibit wavelike banded mode, involving a complex range of processes. Several case studies have been conducted to examine the formation mechanism of these convective banded structures in MCSs. For instance, Luo et al. (2014) proposed a two-scale convective organizational modes that exhibit distinct training effects within a system containing banded convection. Their study highlighted a possible linkage between a mesoscale cold pool and the nocturnal convective initiation, which can lead to the development of multiple parallel rain bands (MPRBs) within an MCS. Furthermore, terrain can significantly influence the development of banded convection, with parallel mountain valleys or gaps playing a controlling role in the formation of MPRBs by enhancing the cold-warm airflow interaction (Q. Wang et al., 2021). A statistical analysis by P. Wang and Meng (2023) further investigated the characteristics of MPRBs. These special organizations in MCSs exhibit a similar banded pattern with convective bands. The statistical features of wavelike banded convection associated with ducted gravity waves may exhibit wave-related characteristics such as horizontal wavelengths, periods, and intrinsic speeds that are consistent with typical gravity waves. These features may not be observed in MPRBs within an MCS.

While there have been case studies on the mechanisms behind wavelike banded convection associated with ducted gravity waves in South China, a comprehensive understanding remains unclear. Du and Zhang (2019) documented a case of banded convective activities near the southern coast of China, where convective bands were found to be closely related to an episode of mesoscale gravity waves. This case suggested a strong interaction between convection and gravity waves. However, the general characteristics (e.g., the spatial and temporal distribution) of wavelike banded convection associated with ducted gravity waves in southern China remain unknown.

Our study represents a multi-year analysis of wavelike banded convection associated with ducted gravity waves in southern China from 2013 to 2021. We aim to answer two key questions: (a) Are there discernible differences between wavelike convective bands with and without the wave duct? (b) What are the specific characteristics of wavelike banded convection with the wave duct, such as wavelength, period, intrinsic phase speed, and their environmental features and locations? The data and the method are introduced in Section 2. The temporal and spatial distribution is presented in Section 3, and the specific characteristics of wavelike banded convection associated with ducted gravity waves are displayed in Section 4. The summary and the discussion are provided in Section 5.

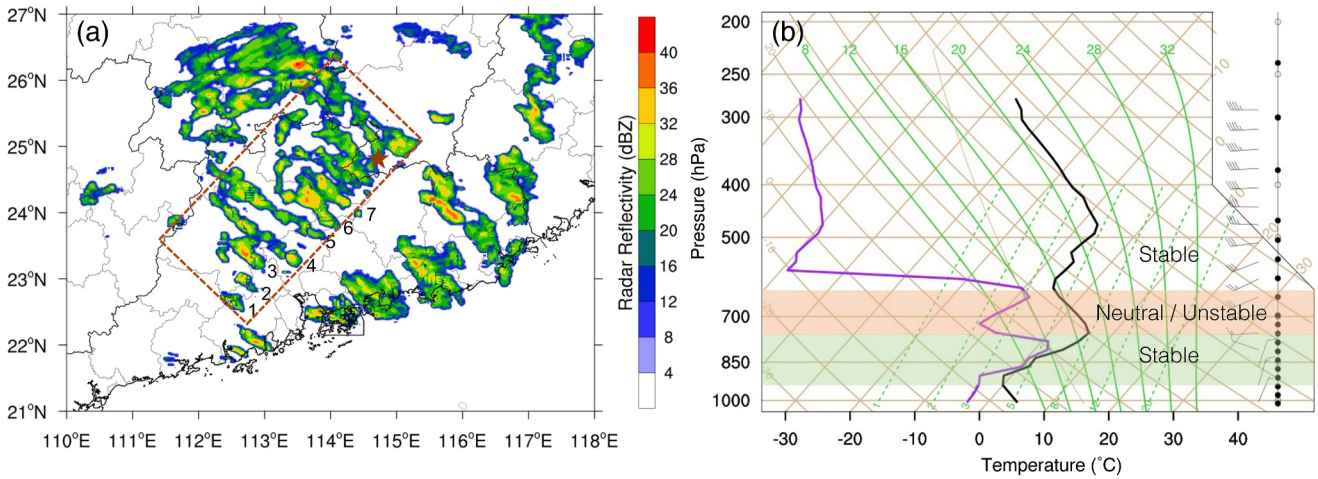

Figure 1. Identification of wavelike banded convection. (a) An example case of wavelike banded convection in southern China. The shading indicates the basic reflectivity reproduced from the radar mosaic maps. (b) Skew T-log p diagram at the location which is the closest to the center of wavelike banded convective marked as the red star in (a).

2. Data and Method

2.1. Data

We utilize radar mosaic maps of basic reflectivity over southern China, produced by the National Meteorological Center of China Meteorological Administration (CMA), spanning from January 2013 to October 2021. We define southern China geographically as the region spanning 20–28°N latitude and 105–121°E longitude. The basic reflectivity value for each range and azimuth bin is optimally selected from the lowest three elevation angles (i.e., 0.5°, 1.5°, and 2.4°), which is also called a "terrain-based hybrid scan" (Bai et al., 2020; Fulton et al., 1998). These maps are generated in real time every 10 min since September 18, 2008 (Meng et al., 2013). From 15 June 2016, the temporal resolution of the radar mosaic maps further increases to every 6 min (Bai et al., 2020).

Additionally, we use radiosonde data from southern China to obtain vertical profiles of relevant atmospheric variables. For synoptic conditions, we rely on the European Center for Medium-Range Weather Forecasts (ECMWF) ERA5 reanalysis data set (Hersbach et al., 2020) with a spatial resolution of 0.25° × 0.25°.

2.2. Identification of Wavelike Banded Convection

The identification of wavelike banded convection follows the methodology outlined by P. Wang and Meng (2023), with adaptations based on the occurrence of ducted gravity waves. Four conditions are used to detect wavelike banded convection.

1. Unlike the criteria for radar reflectivity (>40 dBZ) used for MCS in P. Wang and Meng (2023), we require it to be just greater than 20 dBZ to meet the general convective organization without needing to meet the standard of MCS, as the banded convection is generally moderate (Du & Zhang, 2019).
2. To ensure that the convective organization can be considered as banded, its aspect ratio must be greater than 2.
3. The angle between two adjacent convective bands must be less than 10° to guarantee that the wavelike convective bands are sufficiently parallel.
4. There must be at least 3 convective bands coexisting for over 30 min.

When all the four conditions are met, this indicates the start of a banded convective event, and the event ends when any of these conditions is no longer satisfied. Bands with similar wavelength and phase are treated as part of the same event. If multiple convective bands appear simultaneously in southern China but differ in spatial distribution or phase coherence, they are categorized as separate wavelike banded convective events.

Figure 1a illustrates an example of the wavelike banded convection meeting above criteria. Note that a more practical approach to identifying wavelike banded convection associated with ducted gravity waves is to examine whether a wave duct exists in the environment. However, determining the presence of the "wave-CISK"

mechanism remains challenging due to the lack of an objective method for a multi-year observational investigation, even though there are signatures and evidence of wave-convection interactions as highlighted in the case study of Du and Zhang (2019) with the aid of numerical simulations. Additionally, to verify the existence of ducting structure against the conceptual model in Lindzen and Tung (1976), we examine soundings from the nearest station to the center of the convective bands. It is noted that the nearest sounding station may not fully capture the environmental conditions in some events due to potential representation errors. However, by comparing ERA5 soundings with station observations, we found that these stations effectively characterize the stratification structure of the areas where wavelike banded convection occurs. The ducting structure includes a lower stable layer, a neutral and/or conditionally unstable middle layer, and a stable layer above (Figure 1b). In our study, we refer to the lower stable layer in the three-layer ducting structure as the "low-level stable layer". To identify stability or instability, we compare the lapse rate of an environmental layer (γ) and the moist adiabatic lapse rate (Γ_s). The moist adiabatic lapse rate is calculated by the below equation (Stull, 2017):

$$\Gamma_s = \frac{\Delta T}{\Delta P} = \left[\frac{a \cdot T + c \cdot r_s}{P \cdot \left[1 + \left(b \cdot \frac{r_s}{T^2} \right) \right]} \right] \tag{1}$$

where r_s is mixing ratio, $a = 0.28571$, $b = 1.35 \times 10^7$ K^2, and $c = 2{,}488.4$ K. If $\gamma < \Gamma_s$, the layer is absolutely stable. Otherwise, if $\gamma \geq \Gamma_s$, then the layer is neutral or unstable. As shown in Figure 1b, a three-layer structure is evident, with the green shaded part representing a low-level stable layer overlapped by an unstable or/and neutral layer shown by orange shading. Using this additional procedure, all identified events are further classified into two types of wavelike banded convection: the Bands-WaveDuct type that has the wave ducting stratification condition supporting ducted gravity waves, and the Bands-nonWaveDuct type not meeting the wave ducting conditions.

3. Temporal-Spatial Distribution

A total of 112 wavelike banded convection events are identified during 2013–2021. Among these, 42 events (i.e., 37.5% of all events) are considered as the Bands-WaveDuct type, while the Bands-nonWaveDuct type account for 62.5% (i.e., 70 events in total). A pronounced monthly variation is observed in both types of wavelike banded convection (Figure 2a). The occurrences of the Bands-WaveDuct type are confined from December to April (winter to mid-spring), whereas the Bands-nonWaveDuct type is prevalent year-round, especially from late spring to midsummer (May to July). The occurrences of the Bands-nonWaveDuct type reach a broad minimum from early fall to early winter (September–December).

Diurnal variation also reveals distinct patterns between the two types (Figure 2b). The Bands-WaveDuct type primarily occurs between 00:00 and 04:00 BJT (Beijing Time = UTC+8 hr). The formation of Bands-WaveDuct type at night can be attributed to enhanced radiative cooling, which creates a more stable environment conducive to wave ducting phenomena. Conversely, the Bands-nonWaveDuct type is more prevalent between 16:00 and 20:00 local time. This phenomenon is partly due to increased convective activity in the afternoon and the training effect by the cold pool within organized MCS, which can cause banded convection (Li et al., 2021; Liu et al., 2018; Luo et al., 2014; H. Wang et al., 2014).

Figures 2c and 2d further compare the duration and the convective band numbers between the two types, respectively. The Bands-WaveDuct type generally exhibits longer durations, with a higher proportion lasting above 5 hr. In contrast, the Bands-nonWaveDuct type tends to be shorter-lived, mostly lasting 2–3 hr. Moreover, the Bands-WaveDuct type contains more convective bands compared to the Bands-nonWaveDuct type. A large number of the Bands-WaveDuct events have 7 or more convective bands, accounting for nearly 59.5% of this type, with an average number of 7. In contrast, the Bands-nonWaveDuct events mostly have 4 convective bands, accounting for 37.1%, with an average number of 5.

The spatial distribution characteristics between the two types are compared in Figures 2e and 2f. The Bands-WaveDuct type occurs more frequently along the coastal areas of Fujian Province, in the central and coastal Guangdong Province, and in the northern Guangxi Province (Figure 2e). Conversely, the Bands-nonWaveDuct type tends to occur more often over inland areas (Figure 2f). Geographically, the Bands-WaveDuct type is

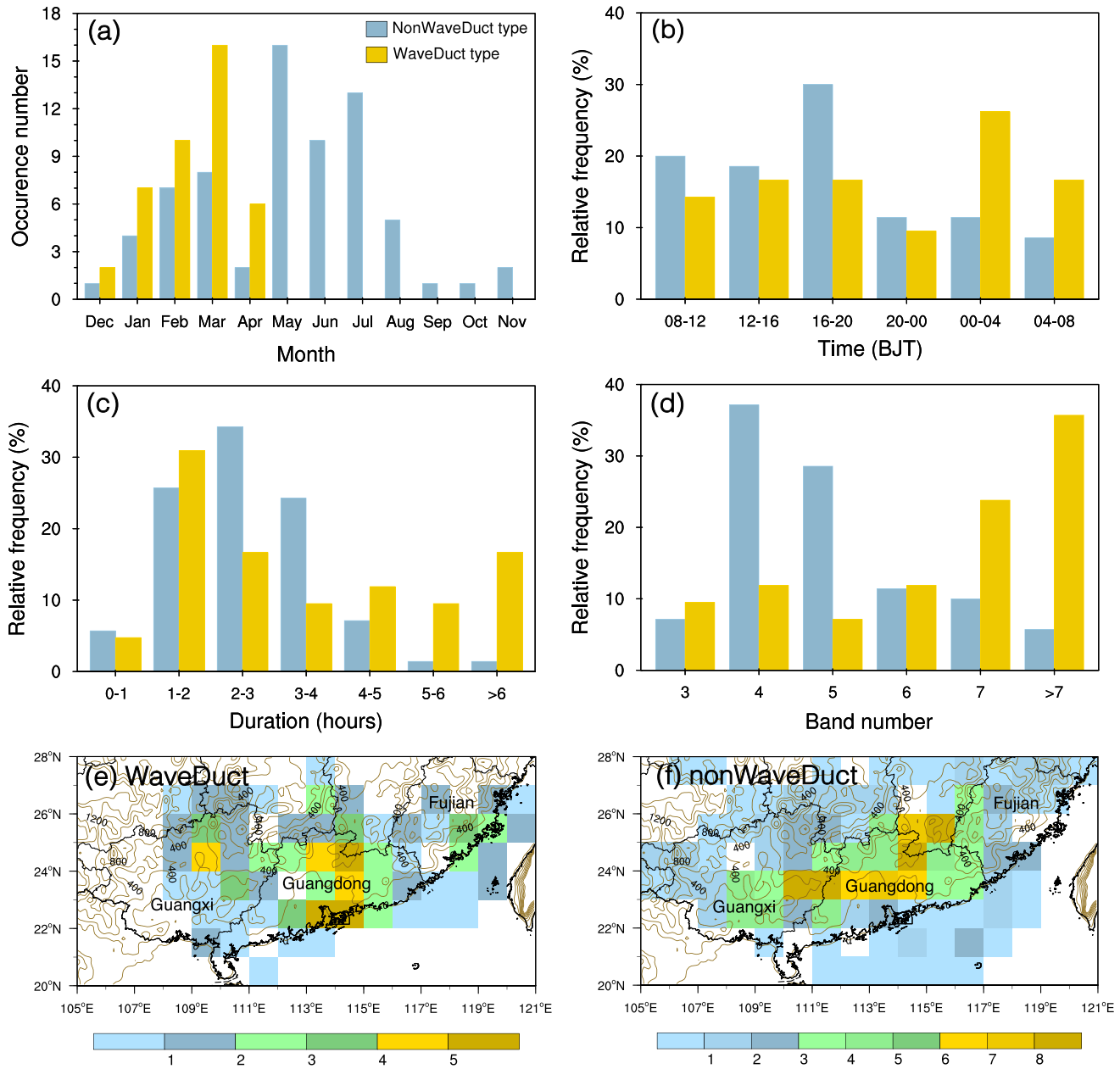

Figure 2. (a) The occurrence number of the Bands-WaveDuct type and the Bands-nonWaveDuct type by month. The frequency (%) normalized by the total occurrence number for each of the two types, categorized by (b) time of day, (c) duration, and (d) band numbers. (e)–(f) Geographical distribution of the frequency of (e) the Bands-WaveDuct type, and (f) the Bands-nonWaveDuct type. The terrain (contoured from 0 to 1,400 m at an interval of 200 m) is represented in the (e) and (f). Banded convective events during 2013–2021 are binned in 1° × 1° grid boxes. The diurnal and spatial distributions are calculated based on the initial timing and location when all four conditions are first satisfied, marking the onset of the event.

more prevalent in regions with topographic elevations. The drier lower troposphere over inland regions could contribute to the occurrence of Bands-nonWaveDuct, as enhanced precipitation evaporation can induce a stronger cold pool. Additionally, other factors such as terrain-induced flow patterns and local wind shear may also contribute to the development of these wavelike convective bands (Luo et al., 2014; Q. Wang et al., 2021). Due to the land-sea contrast, coastal areas typically experience lower temperature than inland areas at night, promoting a more stable lower atmosphere and thus the occurrence of Bands-WaveDuct type.

4. Wavelike Characteristics and Environment Conditions

Since horizontally propagating long-lived mesoscale gravity waves require support from the stratification structure of wave ducting (Koch et al., 1988, 2001; Kusunoki et al., 2000; Powers & Reed, 1993; Ralph et al., 1993; Zhang et al., 2001), we further focus on the Bands-WaveDuct type, where the coupling of convection and gravity waves is likely to occur. We examine their horizontal wavelengths, intrinsic phase speeds, lengths of individual bands, and periods (Figures 3a–3d). The Bands-WaveDuct type mainly exhibits horizontal wavelengths of 30–40 km, periods of 0.5–1.0 hr, and intrinsic phase speeds of 12–15 m s^{-1}. The length of an individual band mainly ranges from 100 to 200 km (Figure 3c), resulting in a relatively wide range of weather impacts. The bands generally replicate many notable characteristics of the long-lived lower tropospheric gravity waves reviewed in Uccellini and Koch (1987) based on 13 observational cases, which are characterized by horizontal wavelengths ranging from ∼50 to 500 km, periods ranging from a few minutes to a few hours, and phase speeds of 10–50 m s^{-1}. Note that the horizontal wavelengths observed here are generally shorter than those described by Uccellini and Koch (1987). Topography might be a factor for the difference in wavelength, as the relatively flat terrain in the U.S contrasts with the rugged terrain in southern China. Additionally, variations in observation data and identification methods could also explain the discrepancies in measured wavelengths between the two studies. These differences may also be due to varying wave source mechanisms and/or wave propagating environments in the different regions.

Propagation speed and movement direction of the convective bands are displayed in Figure 3e. They primarily propagate northeastward at speeds of 10–20 m s^{-1}, although occasionally northwestward at slower speeds of 5–10 m s^{-1}. Since ducted gravity waves primarily propagate within the ducting layer, the composite synoptic background in Figure 4b indicates that the 850-hPa winds over southern China are southwesterly, which may influence the propagation direction of the Bands-WaveDuct type convection. According to Lindzen and Tung (1976), a sufficiently thick stable ducting layer is required to accommodate at least a quarter of the vertical wavelength corresponding to the observed phase speed. The depth of the ducting layer determines the phase speed of the gravity wave through the following equation:

$$C_{d,n} = \frac{N_m D}{\pi\left(\frac{1}{2} + n\right)}, n = 0,1,2,\ldots \tag{2}$$

where n indicates different vertical modes, $C_{d,n}$ is the intrinsic ducted wave phase speed, D is the depth of the low-level stable layer (i.e., the ducting layer), and N_m is the moist Brunt–Väisälä frequency. N_m has different formulas depending on whether or not the air is saturated (Du & Zhang, 2019; Durran & Klemp, 1982). In our calculation, $n = 0$ means the longest vertical wavelength and dominant wavelength, with a quarter of the wavelength fitting D (Lindzen & Tung, 1976).

Based on the positive linear correlation between $C_{d,n}$ and D from Equation 2, we conduct statistical analysis to examine the relationship between the movement speeds of wavelike bands relative to background wind (corresponding to the intrinsic phase speed of gravity waves) and the depth of ducting layer for all Bands-WaveDuct events. As expected, Figure 3f clearly shows a significant positive linear relationship, with a correlation coefficient of 0.70, statistically significant at the 99% confidence level.

Next, we further investigate the synoptic background circulations and environments associated with the Bands-WaveDuct type (Figures 4a and 4b). The composite pattern shows a westerly jet at 500 hPa and a northeast-southwest oriented shear line at 850 hPa, with both located northwest of the bands. These banded convective activities are predominantly found on the cold side of the surface cold front. The atmospheric at 950 hPa is moist and nearly saturated, promoting the convective development. The composite results are in broad agreement with the signatures identified in the case study of Du and Zhang (2019), which are generally common to occurrences of wavelike banded convection associated with ducted gravity waves. We also examined the synoptic background circulations and environmental conditions of the Bands-WaveDuct type across different months and high-frequency regions (not shown) and found them to be generally consistent with the composite synoptic background.

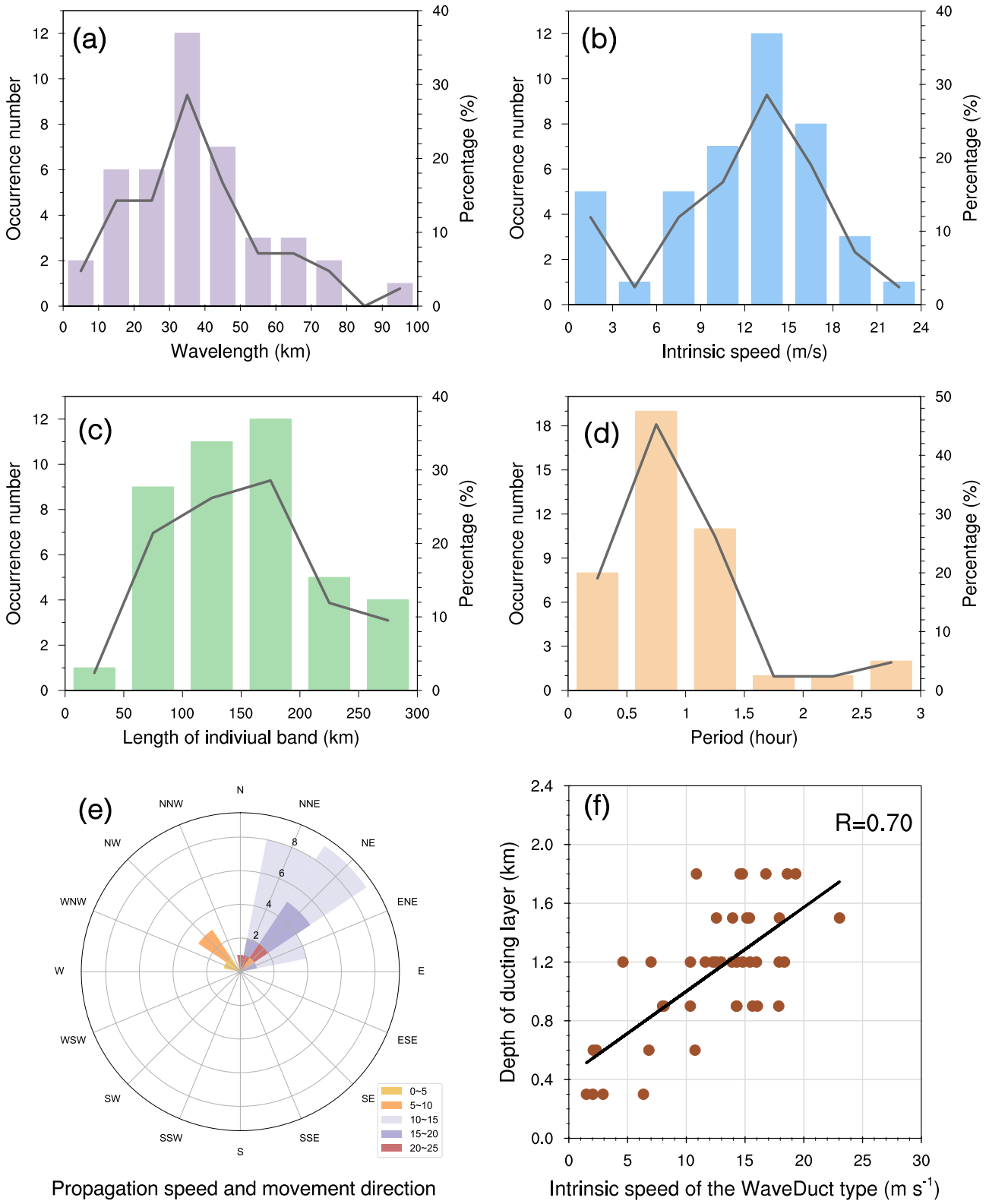
(a)
Occurrence number
Percentage (%)
Wavelength (km)
(b)
Occurrence number
Percentage (%)
Intrinsic speed (m/s)
(c)
Occurrence number
Percentage (%)
Length of indiviual band (km)
(d)
Occurrence number
Percentage (%)
Period (hour)
(e)
N
NNW
NNE
NW
NE
WNW
ENE
W
E
WSW
ESE
SW
SE
SSW
SSE
S
0~5
5~10
10~15
15~20
20~25
Propagation speed and movement direction
(f)
R=0.70
Depth of ducting layer (km)
Intrinsic speed of the WaveDuct type (m s-1)

Figure 3.

As anticipated, the composite vertical thermal profile associated with the Bands-WaveDuct events (Figure 4c) also exhibits a three-layer structure characterized by varying static stability based on N_m: the low-level stable layer is capped by the middle-level less stable layer, which is overlaid by an aloft stable layer, consistent with the wave ducting theory of Lindzen and Tung (1976). Furthermore, we examine other criteria of wave duct highlighted in Lindzen and Tung (1976), including a critical level and small Richardson number (R_i) around the critical level. Here, the critical level refers to a level where the ground-relative phase speed of the wave equals the background wind speed in the wave propagation direction. Based on the statistical results mentioned above, the ground-based phase speed is primarily in the range of 12–15 m s^{-1}, as indicated in Figure 4c by the orange shading areas, which represent the range between these two speeds for the potential existence of the critical level. Using the composite vertical thermal and wind (U) profile, we calculate R_i within these levels:

$$R_i = \frac{N_m^2}{\left(\frac{\partial \overline{U}}{\partial z}\right)^2} \tag{3}$$

In the shading areas, R_i ranges from 0.14 to 0.25. Therefore, the critical levels with small Richardson number around are located in the less stable mid-level layer (Figure 4c). Such stratification conditions allow gravity waves to propagate horizontally in the wave duct for a long period of time without significant energy leaking, facilitating the coupling of convection and gravity waves.

5. Conclusions

This study provides a comprehensive examination of the climatology of wavelike banded convection in southern China, using operational radar mosaic maps, radiosondes, and ERA5 reanalysis data from 2013 to 2021. It documents a first multi-year analysis of the frequency and distribution of wavelike banded convection related to ducted gravity waves. The investigation was originally motivated by a case study of long-lasting banded convective activities resulting from the interaction between convection and gravity waves, as reported by Du and Zhang (2019) and Du et al. (2021) in the same region.

Key findings and broader implications of this study are summarized as follows.

1. A total of 112 cases of wavelike banded convection are identified using radar mosaic maps. These convective bands are categorized into two types: Bands-WaveDuct (associated with ducted gravity waves) and Bands-nonWaveDuct (with no apparent vertical duct structure), based on whether they meet ducting stratification conditions. Nearly one-third of all cases are identified as the Bands-WaveDuct type.
2. Bands-WaveDuct events are predominantly observed during winter and spring (December to April), while Bands-nonWaveDuct events are most frequent in summer and autumn (May to July). Diurnally, the Bands-WaveDuct type peaks between 00:00 and 04:00 BJT, whereas the Bands-nonWaveDuct type peaks between 16:00 and 20:00 BJT. The Bands-WaveDuct type generally has longer durations with a higher proportion lasting over 5 hr and exhibits a larger number (mostly over 6) of convective bands, compared to the Bands-nonWaveDuct type. This difference is possibly due to lower nighttime surface temperature from December to April, which enhances lower-tropospheric static stability and ducting potential for the Bands-WaveDuct type.
3. The Bands-WaveDuct type has a higher frequency along the coastal areas of Fujian Province, the central and coastal parts of Guangdong Province, and northern Guangxi Province. Conversely, the Bands-nonWaveDuct type tends to occur more frequently in inland regions.
4. The Bands-WaveDuct type exhibits characteristics reminiscent of gravity waves, as reported by Uccellini and Koch (1987), including wavelengths ranging from 30 to 40 km, intrinsic phase speeds of 12–15 m s^{-1}, and periods of 0.5–1.0 hr. The length of each individual band typically spans 100–200 km.

Figure 3. (a)–(d) Wavelike characteristics of the Bands-WaveDuct type: (a) horizontal wavelength, (b) intrinsic phase speed, (c) length of individual band, and (d) period. The horizontal wavelength refers to the average distance between two adjacent convective bands. Intrinsic phase speed represents the speed of the gravity wave phase line relative to the background wind speed within the ducting layer, along the horizontal wavenumber vector. The length of individual bands describes the spatial extent of a single convective band at its maximum development. Period refers to the time between successive appearances of banded convection at the same location. (e) Wind rose diagram illustrates the direction and the speed (unit: m s^{-1}) of the propagation of the Bands-WaveDuct type relative to background winds. (d) Scatter diagram shows the relationship between the depth of the ducting layer and the intrinsic phase speed of wavelike bands.

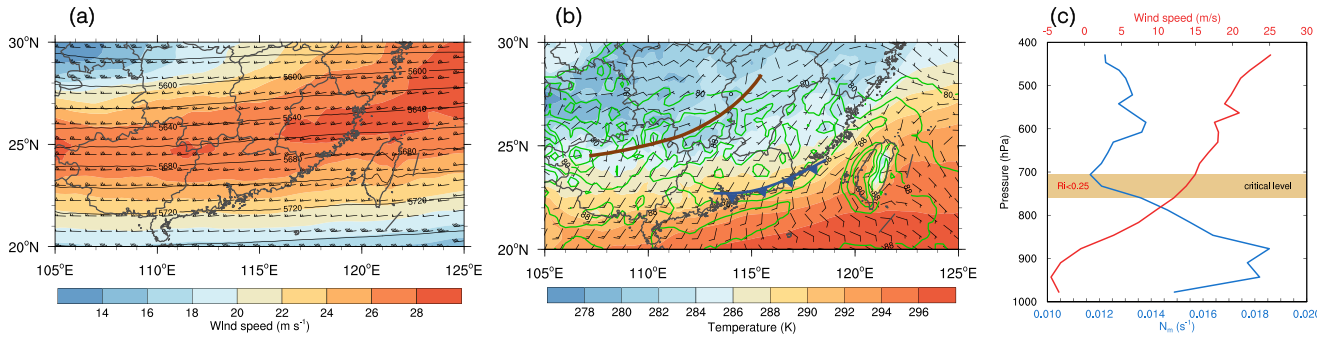

Figure 4. Composite synoptic background circulations for all Bands-WaveDuct events using ERA5 reanalysis. (a) The geopotential height (gpm; contours), wind speed (m s^{-1}; shading), and horizontal wind barbs at 500 hPa; (b) the relative humidity at 950 hPa (%; green contours), surface temperature (K; shading), and horizontal wind barbs at 850 hPa. The solid brown line indicates the 850-hPa shear line, and the surface cold front is marked on the map. (c) Composite vertical profile of the moist Brunt–Väisälä frequency (blue line) and horizontal wind speed along the propagation directions of the convective bands (red line) for Bands-WaveDuct events.

5. Most Bands-WaveDuct events propagate northeastward at speeds of 12–15 m s^{-1}. According to wave ducting theory, intrinsic phase speed is determined by the strength and depth of the low-level stable layer $\left(C_{d,n} = \frac{N_m D}{\pi\left(\frac{1}{2}+n\right)}\right)$. The positive correlation between the depth of low-level stable layer and intrinsic phase speed found in our statistics provides further quantitative support for wave ducting theory.
6. The occurrence of Bands-WaveDuct events is closely related to the background circulation patterns, often featuring a westerly jet at 500 hPa located northwest and a position to the cold side of the surface cold front, enhancing the stable layer in the lower troposphere necessary for ducted gravity waves. Analysis of the composite vertical structure of moist Brunt–Väisälä frequency reveals a distinct pattern: the low-level stable layer capped by a less-stable reflecting layer with a critical level where the Richardson number is less than 1/4.

This study does not address the reasons for the preferred locations of wavelike banded convection related to ducted gravity waves, which will be interesting to explore in future work. Additionally, we will conduct similar statistical studies over other regions of China and compare their similarities and differences. High-resolution observations and cloud-permitting numerical simulations for multiple cases will further enhance our understanding of the detailed factors involved in different regions. Since high-resolution surface pressure observations can provide more direct evidence of ducted gravity wave occurrences (e.g., Koch & O'Handley, 1997; Ruppert & Bosart, 2014), we will focus on collecting and analyzing these data to enhance the investigation of these waves.

Data Availability Statement

The ERA5 reanalysis data (Hersbach et al., 2020) used in this study are publicly available from the Copernicus Data Store (CDS) (Hersbach et al., 2023a, Hersbach et al., 2023b). The radar mosaic maps of all identified wavelike banded convective events are achieved at Zhou (2024).

Acknowledgments
This study was supported by the National Natural Science Foundation of China (Grants 42122033, 42375003, 42075005, and 42075006), the Science and Technology Planning Project of Guangdong Province (Grants 2023B1212060019 and 2020B1212060025), the Innovation Group Project of Southern Marine Science and Engineering Guangdong Laboratory (Zhuhai) (No. 316323005), the Key Innovation Team of China Meteorological Administration (CMA2023ZD08). We also acknowledge the high-performance computing support from School of Atmospheric Sciences of Sun Yat-sen University.

References

Alexander, M. J., Holton, J. R., & Durran, D. R. (1995). The gravity wave response above deep convection in a squall line simulation. *Journal of the Atmospheric Sciences*, *52*(12), 2212–2226. https://doi.org/10.1175/1520-0469(1995)052<2212:TGWRAD>2.0.CO;2

Bai, L., Chen, G., & Huang, L. (2020). Image processing of radar mosaics for the climatology of convection initiation in south China. *Journal of Applied Meteorology and Climatology*, *59*(1), 65–81. https://doi.org/10.1175/JAMC-D-19-0081.1

Bosart, L. F., Bracken, W. E., & Seimon, A. (1998). A study of cyclone mesoscale structure with emphasis on a large-amplitude inertia–gravity wave. *Monthly Weather Review*, *126*(6), 1497–1527. https://doi.org/10.1175/1520-0493(1998)126<1497:ASOCMS>2.0.CO;2

Bosart, L. F., & Cussen, J. P. (1973). Gravity wave phenomena accompanying east coast cyclogenesis. *Monthly Weather Review*, *101*(5), 446–454. https://doi.org/10.1175/1520-0493(1973)101<0446:GWPAEC>2.3.CO;2

Bretherton, C. (1988). Group velocity and the linear response of stratified fluids to internal heat or mass sources. *Journal of the Atmospheric Sciences*, *45*(1), 81–94. https://doi.org/10.1175/1520-0469(1988)045<0081:GVATLR>2.0.CO;2

Chen, Z., & Du, Y. (2024). The influence of topography on the diurnal rainfall propagation in the Bay of Bengal. *Journal of the Atmospheric Sciences*, *81*(6), 1019–1032. https://doi.org/10.1175/JAS-D-23-0225.1

Clarke, R. H. (1972). The morning glory: An atmospheric hydraulic jump. *Journal of Applied Meteorology*, *11*(2), 304–311. https://doi.org/10.1175/1520-0450(1972)011<0304:TMGAAH>2.0.CO;2

Du, Y. (2023). Offshore migration of summer monsoon low-level jet on a diurnal scale. *Geophysical Research Letters*, *50*(20), e2023GL103840. https://doi.org/10.1029/2023GL103840

Du, Y., & Rotunno, R. (2015). Thermally driven diurnally periodic wind signals off the east coast of China. *Journal of the Atmospheric Sciences*, *72*(7), 2806–2821. https://doi.org/10.1175/JAS-D-14-0339.1

Du, Y., & Rotunno, R. (2018). Diurnal cycle of rainfall and winds near the south coast of China. *Journal of the Atmospheric Sciences*, *75*(6), 2065–2082. https://doi.org/10.1175/JAS-D-17-0397.1

Du, Y., Rotunno, R., Chen, Z., & Yang, H. (2024). A linear theory for periodic convectively forced gravity waves near a coastline. *Journal of the Atmospheric Sciences*, *81*(7), 1271–1288. https://doi.org/10.1175/JAS-D-23-0173.1

Du, Y., Rotunno, R., & Zhang, F. (2019). Impact of vertical wind shear on gravity wave propagation in the land–sea-breeze circulation at the equator. *Journal of the Atmospheric Sciences*, *76*(10), 3247–3265. https://doi.org/10.1175/JAS-D-19-0069.1

Du, Y., & Zhang, F. (2019). Banded convective activity associated with mesoscale gravity waves over southern China. *Journal of Geophysical Research: Atmospheres*, *124*(4), 1912–1930. https://doi.org/10.1029/2018JD029523

Du, Y., Zhang, F., Sun, Y. Q., Wei, J., & Li, X. (2021). Practical and intrinsic predictability of wave-convection coupled bands over southern China. *Journal of Geophysical Research: Atmospheres*, *126*(22), e2021JD034882. https://doi.org/10.1029/2021JD034882

Durran, D. R., & Klemp, J. B. (1982). On the effects of moisture on the Brunt-Väisälä frequency. *Journal of the Atmospheric Sciences*, *39*(10), 2152–2158. https://doi.org/10.1175/1520-0469(1982)039<2152:OTEOMO>2.0.CO;2

Fang, J., & Du, Y. (2022). A global survey of diurnal offshore propagation of rainfall. *Nature Communications*, *13*(1), 7437. https://doi.org/10.1038/s41467-022-34842-0

Fulton, R. A., Breidenbach, J. P., Seo, D.-J., Miller, D. A., & O'Bannon, T. (1998). The WSR-88D rainfall algorithm. *Weather and Forecasting*, *13*(2), 377–395. https://doi.org/10.1175/1520-0434(1998)013<0377:TWRA>2.0.CO;2

Hersbach, H., Bell, B., Berrisford, P., Biavati, G., Horányi, A., Muñoz-Sabater, J., et al. (2023a). ERA5 hourly data on pressure levels from 1940 to present [Dataset]. *Copernicus Climate Change Service (C3S) Climate Data Store (CDS)*. https://doi.org/10.24381/CDS.BD0915C6

Hersbach, H., Bell, B., Berrisford, P., Biavati, G., Horányi, A., Muñoz-Sabater, J., et al. (2023b). ERA5 hourly data on single levels from 1940 to present [Dataset]. *Copernicus Climate Change Service (C3S) Climate Data Store (CDS)*. https://doi.org/10.24381/CDS.ADBB2D47

Hersbach, H., Bell, B., Berrisford, P., Hirahara, S., Horányi, A., Muñoz-Sabater, J., et al. (2020). The ERA5 global reanalysis. *Quarterly Journal of the Royal Meteorological Society*, *146*(730), 1999–2049. https://doi.org/10.1002/qj.3803

Koch, S. E., Golus, R. E., & Dorian, P. B. (1988). A mesoscale gravity wave event observed during CCOPE. Part II: Interactions between mesoscale convective systems and the antecedent waves. *Monthly Weather Review*, *116*(12), 2545–2569. https://doi.org/10.1175/1520-0493(1988)116<2545:AMGWEO>2.0.CO;2

Koch, S. E., & O'Handley, C. (1997). Operational forecasting and detection of mesoscale gravity waves. *Weather and Forecasting*, *12*(2), 253–281. https://doi.org/10.1175/1520-0434(1997)012<0253:OFADOM>2.0.CO;2

Koch, S. E., Zhang, F., Kaplan, M. L., Lin, Y.-L., Weglarz, R., & Trexler, C. M. (2001). Numerical simulations of a gravity wave event over CCOPE. Part III: The role of a mountain–plains solenoid in the generation of the second wave episode. *Monthly Weather Review*, *129*(5), 909–933. https://doi.org/10.1175/1520-0493(2001)129<0909:NSOAGW>2.0.CO;2

Koppel, L. L., Bosart, L. F., & Keyser, D. (2000). A 25-yr climatology of large-amplitude hourly surface pressure changes over the conterminous United States. *Monthly Weather Review*, *128*(1), 51–68. https://doi.org/10.1175/1520-0493(2000)128<0051:AYCOLA>2.0.CO;2

Kusunoki, K., Eito, H., & Akaeda, K. (2000). A case study of low-level internal gravity waves using Doppler radar and ACARS. *Journal of the Meteorological Society of Japan. Ser. II*, *78*(5), 511–525. https://doi.org/10.2151/jmsj1965.78.5_511

Lane, T. P., & Zhang, F. (2011). Coupling between gravity waves and tropical convection at mesoscales. *Journal of the Atmospheric Sciences*, *68*(11), 2582–2598. https://doi.org/10.1175/2011JAS3577.1

Li, H., Huang, Y., Hu, S., Wu, N., Liu, X., & Xiao, H. (2021). Roles of terrain, surface roughness, and cold pool outflows in an extreme rainfall event over the coastal region of south China. *Journal of Geophysical Research: Atmospheres*, *126*(23), e2021JD035556. https://doi.org/10.1029/2021JD035556

Lin, Y.-L., & Chun, H.-Y. (1991). Effects of diabatic cooling in a shear flow with a critical level. *Journal of the Atmospheric Sciences*, *48*(23), 2476–2491. https://doi.org/10.1175/1520-0469(1991)048<2476:EODCIA>2.0.CO;2

Lin, Y.-L., & Goff, R. C. (1988). A study of a mesoscale solitary wave in the atmosphere originating near a region of deep convection. *Journal of the Atmospheric Sciences*, *45*(2), 194–206. https://doi.org/10.1175/1520-0469(1988)045<0194:ASOAMS>2.0.CO;2

Lin, Y. L., & Smith, R. B. (1986). Transient dynamics of airflow near a local heat source. *Journal of the Atmospheric Sciences*, *43*(1), 40–49. https://doi.org/10.1175/1520-0469(1986)043<0040:TDOANA>2.0.CO;2

Lindzen, R. S. (1974). Wave-CISK in the tropics. *Journal of the Atmospheric Sciences*, *31*(1), 156–179. https://doi.org/10.1175/1520-0469(1974)031<0156:WCITT>2.0.CO;2

Lindzen, R. S., & Tung, K.-K. (1976). Banded convective activity and ducted gravity waves. *Monthly Weather Review*, *104*(12), 1602–1617. https://doi.org/10.1175/1520-0493(1976)104<1602:BCAADG>2.0.CO;2

Liu, X., Luo, Y., Guan, Z., & Zhang, D. (2018). An extreme rainfall event in coastal south China during SCMREX-2014: Formation and roles of rainband and echo trainings. *Journal of Geophysical Research: Atmospheres*, *123*(17), 9256–9278. https://doi.org/10.1029/2018jd028418

Luo, Y., Gong, Y., & Zhang, D.-L. (2014). Initiation and organizational modes of an extreme-rain-producing mesoscale convective system along a mei-yu front in East China. *Monthly Weather Review*, *142*(1), 203–221. https://doi.org/10.1175/MWR-D-13-00111.1

Meng, Z., Yan, D., & Zhang, Y. (2013). General features of squall lines in east China. *Monthly Weather Review*, *141*(5), 1629–1647. https://doi.org/10.1175/MWR-D-12-00208.1

Powers, J. G. (1997). Numerical model simulations of a mesoscale gravity wave event: Sensitivity tests and spectral analyses. *Monthly Weather Review*, *125*(8), 1838–1869. https://doi.org/10.1175/1520-0493(1997)125<1838:NMSOAM>2.0.CO;2

Powers, J. G., & Reed, R. J. (1993). Numerical simulation of the large-amplitude mesoscale gravity-wave event of 15 December 1987 in the central United States. https://doi.org/10.1175/1520-0493(1993)121<2285:NSOTLA>2.0.CO;2

Ralph, F. M., Venkateswaran, V., & Crochet, M. (1993). Observations of a mesoscale ducted gravity wave. *Journal of the Atmospheric Sciences*, *50*(19), 3277–3291. https://doi.org/10.1175/1520-0469(1993)050<3277:OOAMDG>2.0.CO;2

Raymond, D. J. (1975). A model for predicting the movement of continuously propagating convective storms. *Journal of the Atmospheric Sciences*, *32*(7), 1308–1317. https://doi.org/10.1175/1520-0469(1975)032<1308:AMFPTM>2.0.CO;2

Raymond, D. J. (1984). A wave-cisk model of squall lines. *Journal of the Atmospheric Sciences*, *41*(12), 1946–1958. https://doi.org/10.1175/1520-0469(1984)041<1946:AWCMOS>2.0.CO;2

Raymond, D. J. (1987). A forced gravity wave model of serf-organizing convection. *Journal of the Atmospheric Sciences*, *44*(23), 3528–3543. https://doi.org/10.1175/1520-0469(1987)044<3528:AFGWMO>2.0.CO;2

Rottman, J. W., & Einaudi, F. (1993). Solitary waves in the atmosphere. *Journal of the Atmospheric Sciences*, *50*(14), 2116–2136. https://doi.org/10.1175/1520-0469(1993)050<2116:SWITA>2.0.CO;2

Rotunno, R. (1983). On the linear theory of the land and sea breeze. *Journal of the Atmospheric Sciences*, *40*(8), 1999–2009. https://doi.org/10.1175/1520-0469(1983)040<1999:OTLTOT>2.0.CO;2

Ruppert, J. H., & Bosart, L. F. (2014). A case study of the interaction of a mesoscale gravity wave with a mesoscale convective system. *Monthly Weather Review*, *142*(4), 1403–1429. https://doi.org/10.1175/MWR-D-13-00274.1

Ruppert, J. H., Koch, S. E., Chen, X., Du, Y., Seimon, A., Sun, Y. Q., et al. (2022). Mesoscale gravity waves and midlatitude weather: A tribute to fuqing zhang. *Bulletin of the American Meteorological Society*, *103*(1), E129–E156. https://doi.org/10.1175/BAMS-D-20-0005.1

Starr Malkus, J., & Stern, M. E. (1953). The flow of a stable atmosphere over a heated island, Part I. *Journal of Meteorology*, *10*(1), 30–41. https://doi.org/10.1175/1520-0469(1953)010<0030:TFOASA>2.0.CO;2

Stephan, C. C., Alexander, M. J., Hedlin, M., De Groot-Hedlin, C. D., & Hoffmann, L. (2016). A case study on the far-field properties of propagating tropospheric gravity waves. *Monthly Weather Review*, *144*(8), 2947–2961. https://doi.org/10.1175/MWR-D-16-0054.1

Stull, R. (2017). Water vapor. In *Practical meteorology: An algebra-based survey of atmospheric science (version 1.02b)* (pp. 87–118). Department of Earth, Ocean and Atmospheric Sciences University of British Columbia. Retrieved from https://www.eoas.ubc.ca/books/Practical_Meteorology/st

Sun, W.-Y., & Orlanski, I. (1981). Large mesoscale convection and sea breeze circulation. part i: Linear stability analysis. *Journal of the Atmospheric Sciences*, *38*(8), 1675–1693. https://doi.org/10.1175/1520-0469(1981)038<1675:LMCASB>2.0.CO;2

Tjernström, M., & Mauritsen, T. (2009). Mesoscale variability in the summer arctic boundary layer. *Boundary-Layer Meteorology*, *130*(3), 383–406. https://doi.org/10.1007/s10546-009-9354-x

Uccellini, L. W., & Koch, S. E. (1987). The synoptic setting and possible energy sources for mesoscale wave disturbances. *Monthly Weather Review*, *115*(3), 721–729. https://doi.org/10.1175/1520-0493(1987)115<0721:TSSAPE>2.0.CO;2

Wang, H., Luo, Y., & Jou, B. J. (2014). Initiation, maintenance, and properties of convection in an extreme rainfall event during SCMREX: Observational analysis. *Journal of Geophysical Research: Atmospheres*, *119*(23), 13206–13232. https://doi.org/10.1002/2014jd022339

Wang, P., & Meng, Z. (2023). General features of MCSs with the organization of multiple parallel rainbands in China. *Monthly Weather Review*, *151*(9), 2485–2499. https://doi.org/10.1175/MWR-D-22-0304.1

Wang, Q., Zhang, Y., Zhu, K., Tan, Z., & Xue, M. (2021). A case study of the initiation of parallel convective lines back-building from the south side of a mei-yu front over complex terrain. *Advances in Atmospheric Sciences*, *38*(5), 717–736. https://doi.org/10.1007/s00376-020-0216-2

Wei, J., & Zhang, F. (2014). Mesoscale gravity waves in moist baroclinic jet–front systems. *Journal of the Atmospheric Sciences*, *71*(3), 929–952. https://doi.org/10.1175/JAS-D-13-0171.1

Wei, J., & Zhang, F. (2015). Tracking gravity waves in moist baroclinic jet-front systems. *Journal of Advances in Modeling Earth Systems*, *7*(1), 67–91. https://doi.org/10.1002/2014ms000395

Yang, H., & Du, Y. (2024). Difference between upshear- and downshear-propagating waves associated with the development of squall lines. *Monthly Weather Review*, *152*(6), 1399–1420. https://doi.org/10.1175/MWR-D-23-0109.1

Yang, H., Du, Y., Chen, Z., & Fang, J. (2024). Could developing frontal rainfall influence warm-sector rainfall? *Geophysical Research Letters*, *51*(15), e2024GL110430. https://doi.org/10.1029/2024GL110430

Yang, H., Du, Y., & Wei, J. (2023). Generation of multiple gravity wave couplets from convection. *Journal of the Atmospheric Sciences*, *80*(9), 2323–2343. https://doi.org/10.1175/JAS-D-22-0212.1

Zhang, F. (2004). Generation of mesoscale gravity waves in upper-tropospheric jet–front systems. *Journal of the Atmospheric Sciences*, *61*(4), 440–457. https://doi.org/10.1175/1520-0469(2004)061<0440:GOMGWI>2.0.CO;2

Zhang, F., Davis, C. A., Kaplan, M. L., & Koch, S. E. (2001). Wavelet analysis and the governing dynamics of a large-amplitude mesoscale gravity-wave event along the east coast of the United States. *Quarterly Journal of the Royal Meteorological Society*, *127*(577), 2209–2245. https://doi.org/10.1002/qj.49712757702

Zhou, X. (2024). Radar mosaic maps for wavelike banded convection over southern China (2013-2021) [Dataset]. *Zenodo*. https://doi.org/10.5281/zenodo.13324684